

# High-order gas-kinetic scheme for radiation hydrodynamics in equilibrium-diffusion limit

Yaqing Yang · Liang Pan · Wenjun Sun

Received: date/Accepted: date

**Abstract** In this paper, a high-order gas-kinetic scheme is developed for the equation of radiation hydrodynamics in equilibrium-diffusion limit which describes the interaction between matter and radiation. To recover RHE, the Bhatnagar-Gross-Krook (BGK) model with modified equilibrium state is considered. In the equilibrium-diffusion limit, the time scales of radiation diffusion and hydrodynamic part are different, and it will make the time step very small for the fully explicit scheme. An implicit-explicit (IMEX) scheme is applied, in which the hydrodynamic part is treated explicitly and the radiation diffusion is treated implicitly. For the hydrodynamics part, a time dependent gas distribution function can be constructed by the integral solution of modified BGK equation, and the time dependent numerical fluxes can be obtained by taking moments of gas distribution function. For the radiation diffusion term, the nonlinear generalized minimal residual (GMRES) method is used. To achieve the temporal accuracy, a two-stage method is developed, which is an extension of two-stage method for hyperbolic conservation law. For the spatial accuracy, the multidimensional weighted essential non-oscillation (WENO) scheme is used for the spatial reconstruction. A variety of numerical tests are provided for the performance of current scheme, including the order of accuracy and robustness.

**Keywords** High-order gas-kinetic scheme, equation of radiation hydrodynamics, GMRES method, WENO scheme.

## 1 Introduction

The equation of radiation hydrodynamics describes the radiative transport through a fluid with coupled momentum and energy exchange [21, 6, 23]. Its applications are mainly in high-temperature hydrodynamics, including gaseous stars in astrophysics, supernova explosions, combustion phenomena, reentry vehicles, fusion physics and inertial confinement fusion. The importance of thermal radiation increases as the temperature is raised in the above problems. Such as for the moderate temperature, the role of radiation is primarily one of transporting energy by radiative process.

---

Yaqing Yang  
Laboratory of Mathematics and Complex Systems, School of Mathematical Sciences, Beijing Normal University,  
Beijing, China  
E-mail: yqyangbnu@163.com

Liang Pan  
Laboratory of Mathematics and Complex Systems, School of Mathematical Sciences, Beijing Normal University,  
Beijing, China  
E-mail: panliang@bnu.edu.cn

Wenjun Sun  
Center for Applied Physics and Technology, College of Engineering, Peking University, Beijing, China  
Institute of Applied Physics and Computational Mathematics, Beijing, China  
E-mail: sun\_wenjun@iapcm.ac.cn

But for the higher temperature, the energy and momentum densities of the radiation field may become comparable to or even dominates the corresponding fluid quantities.

In the case of the zero diffusion limit [30,15,29], the equation of radiation hydrodynamics can be written into a nonlinear hyperbolic system of conservation laws. But for the more complicated equilibrium-diffusion limit [9], another nonlinear diffusion term for radiative heat transfer should be added. Due to the highly non-linearity of this radiation diffusion terms, it becomes more challenge to design a high-order and robust numerical method. For the scales of characteristic time between the radiation and hydrodynamics are different by several orders of magnitude, and it usually requires the radiation part to be solved implicitly to guarantee the numerical stability. There are many numerical method for the radiation hydrodynamics in equilibrium-diffusion limit. With the operator splitting method, the Godunov schemes were proposed for the hyperbolic part and an implicit scheme is proposed for the radiative heat transfer [9,1,3]. The only second-order accuracy can be achieved in space and time for both the equilibrium diffusion and streaming limit, and it is also capable of computing radiative shock solutions accurately. Furthermore, to achieve the high-order accuracy, one-dimension implicit-explicit (IMEX) Lagrangian high-order scheme was developed in [8]. The essentially non-oscillatory (ENO) [11] method is used for the advection and radiation diffusion term to obtain the high spatial accuracy, and the strong stability preserving method is used for high order temporal accuracy. The more work on the RHEs' computation can be found in [20,19,16].

In the last decades, the gas-kinetic scheme (GKS) and based on the Bhatnagar-Gross-Krook (BGK) model [2,7] have been developed systematically for the computations from low speed flows to supersonic ones [31,32]. The gas-kinetic scheme is based on an analytical integral solution of the BGK equation, and gas distribution function at a cell interface provides a multi-scale evolution process from the kinetic particle transport to the hydrodynamic wave propagation. With the two-stage fourth-order method for Lax-Wendroff type flow solvers [17,10], the high-order gas-kinetic schemes were developed [22,13]. The high-order scheme not only reduces the complexity of computation, but also improves the accuracy of the numerical solution. Most importantly, the robustness is as good as the second-order shock capturing scheme. Furthermore, with the discretization of particle velocity space, a unified gas-kinetic scheme (UGKS) has been developed for the flow study in entire Knudsen number regimes from rarefied to continuum ones [33,12,18]. Recently, the UGKS is extended to solve radiative transfer system with both scattering and absorption/emission effects [25,26,27]. The asymptotic preserving (AP) property can be accurately recovered. For the equation of radiation hydrodynamics, a multi-scale scheme is developed, in which GKS is used for the compressible inviscid flow and UGKS is used for the non-equilibrium radiative transfer [28]. Due to the possible large variation of fluid opacity in different regions, the transport of photons through the flow system is simulated by the multi-scale scheme.

In this paper, a high-order gas-kinetic scheme is proposed for the equation of radiation hydrodynamic in the equilibrium-diffusion limit. Based on the zeroth-order Chapman-Enskog expansion, the hydrodynamic part of radiation hydrodynamic equation can be obtained from the modified BGK equation with modified equilibrium state. The radiation diffusion term is considered as source term. Since the time scales of radiation diffusion and hydrodynamic part are different and it will make the time step of an explicit scheme very small. Thus, an implicit-explicit (IMEX) scheme is developed for solving the radiation hydrodynamic equation, in which the fluid advection term is treated explicitly and the radiation diffusion is treated implicitly. For the hydrodynamic part, the gas-kinetic solver with the modified equilibrium state is used to solve the compressible flow equations. The nonlinear Newton-GMRES method [24,5] is used to deal with the radiation diffusion. To achieve the temporal accuracy, the two-stage third-order temporal discretization is developed, which is an extension of two-stage method was developed for Lax-Wendroff type flow solvers. To achieve the spatial accuracy, the classical weighted essentially non-oscillatory (WENO) [14,4] method reconstruction is used. With the two-stage temporal discretization and WENO reconstruction, a reliable framework was provided for equation of radiation hydrodynamics. Various numerical experiments are carried out to validate the performance of current scheme.

This paper is organized as follows. In Section 2, the equation of radiation hydrodynamics and corresponding BGK model are introduced. The high-order gas-kinetic for RHE is presented in Section 3. Numerical examples are included in Section 4 and the last section is the conclusion.

## 2 Equation of radiation hydrodynamics and BGK model

### 2.1 Equation of radiation hydrodynamics

The equation of radiation hydrodynamics (RHE) describes the motion of flows under a radiation field. It consists of the Euler equations coupling with the radiation momentum and energy sources and the radiation-transport equation, and can be given as follows

$$\begin{aligned}\frac{\partial \rho}{\partial t} + \nabla \cdot (\rho \mathbf{U}) &= 0, \\ \frac{\partial \rho \mathbf{U}}{\partial t} + \nabla \cdot (\rho \mathbf{U} \mathbf{U} + p) &= -\mathbf{S}_{rp}, \\ \frac{\partial E}{\partial t} + \nabla \cdot ((E + p)\mathbf{U}) &= -S_{re}, \\ \frac{1}{c} \frac{\partial I_\nu}{\partial t} + \boldsymbol{\Omega} \cdot \nabla I_\nu &= Q_\nu,\end{aligned}$$

where  $\rho$ ,  $\mathbf{U}$ ,  $E$  and  $p$  are the density, velocity, total energy and pressure of the matter, respectively.  $\mathbf{S}_{rp}$  is the radiation momentum source,  $S_{re}$  is the radiation energy source,  $c$  is the speed of light,  $I_\nu$  is radiation intensity,  $\boldsymbol{\Omega}$  is the photon direction of flight and  $Q_\nu$  is the angle and frequency dependent radiation source representing the radiation-matter interaction. The radiation-transport equation is essentially the conservation of the photon number, which reveals the relationship between the photon free transport and radiation-matter interaction, i.e. photon emission, photon absorption and photon scatter. The source terms  $S_{re}$  and  $\mathbf{S}_{rp}$  can be written as the zeroth and first order frequency-integrated angular moments of  $Q_\nu$ , respectively,

$$\begin{aligned}S_{re} &\equiv \int_{4\pi} \int_0^\infty Q_\nu d\Omega d\nu = \frac{\partial \varepsilon}{\partial t} + \nabla \cdot \mathcal{F}, \\ \mathbf{S}_{rp} &\equiv \frac{1}{c} \int_{4\pi} \int_0^\infty \boldsymbol{\Omega} Q_\nu d\Omega d\nu = \frac{1}{c^2} \frac{\partial \mathcal{F}}{\partial t} + \nabla \cdot \mathcal{P},\end{aligned}$$

where  $\varepsilon$  is radiation energy density,  $\mathcal{F}$  is radiation flux and  $\mathcal{P}$  is radiation-pressure. The equilibrium-diffusion approximation imposes four basic assumptions to simplify RHE, i.e. the photon mean-free-path is small compared to the size of the absorption-dominated system, the matter-radiation system is in thermal equilibrium, the radiation flux is diffusive, and the radiation pressure is isotropic. It is also assumed that the radiative temperature and the fluid temperature are equal and the gas is radiatively opaque so that the equilibrium diffusion will be dealt with. With the assumptions above, the radiation energy density, radiation flux and radiation-pressure can be simplified as

$$\begin{aligned}\varepsilon &= a_R T^4, \\ \mathcal{F} &= -\kappa \nabla T^4 + \frac{4}{3} \mathbf{U} a_R T^4, \\ \mathcal{P} &= \frac{1}{3} a_R T^4,\end{aligned}$$

where  $T$  is temperature,  $\kappa$  is diffusion constant and  $a_R$  is radiation constant representing the ratio of the radiation energy to the material energy. The time-derivative of radiation flux in the total-momentum can be dropped in accordance with the diffusion approximation. Therefore, the

equation of radiation hydrodynamics in the equilibrium-diffusion limit can be written as

$$\begin{aligned}\frac{\partial \rho}{\partial t} + \nabla \cdot (\rho \mathbf{U}) &= 0, \\ \frac{\partial \rho \mathbf{U}}{\partial t} + \nabla \cdot (\rho \mathbf{U} \mathbf{U} + p^*) &= 0, \\ \frac{\partial E^*}{\partial t} + \nabla \cdot ((E^* + p^*) \mathbf{U}) &= \nabla \cdot (\kappa \nabla T^4),\end{aligned}\tag{1}$$

where the total energy  $E^*$  and the total pressure  $p^*$  are given as

$$\begin{aligned}E^* &= \frac{1}{2} \rho \mathbf{U}^2 + \frac{p}{\gamma - 1} + a_R T^4, \\ p^* &= p + \frac{1}{3} a_R T^4.\end{aligned}$$

The polytropic ideal gas is considered, and the equation of state is given by

$$p = (\gamma - 1) \rho e = (\gamma - 1) \rho c_v T,$$

where  $e$  is the specific internal energy,  $c_v$  is the heat capacity at constant volume and  $\gamma$  is the specific heat ratio.

## 2.2 BGK model

In this paper, a high-order gas-kinetic scheme will be presented for two-dimensional flows. To recover the macroscopic equation of radiation hydrodynamics Eq.(1), the modified BGK equation [2, 7] can be written as

$$f_t + u f_x + v f_y = \frac{g - f}{\tau},\tag{2}$$

where  $f$  is the gas distribution function,  $g$  is the equilibrium distribution,  $\mathbf{u} = (u, v)$  is the particle velocity and  $\tau$  is the collision time. For the equation of radiation hydrodynamics, a modified equilibrium state function is introduced [29]

$$g(\mathbf{x}, \mathbf{u}, t) = \rho \left( \frac{\lambda_1 \lambda_2}{(\lambda_1 + \lambda_2) \pi} \right)^{d/2} \left( \frac{\lambda_1}{\pi} \right)^{K_1/2} \left( \frac{\lambda_2}{\pi} \right)^{K_2/2} e^{-\left( \frac{\lambda_1 \lambda_2}{\lambda_1 + \lambda_2} (\mathbf{u} - \mathbf{U})^2 + \lambda_1 \xi_1^2 + \lambda_2 \xi_2^2 \right)},$$

where  $d = 2$  for two dimensional system,  $\mathbf{U}$  is the macroscopic velocity, the internal variables are defined as  $\xi_1^2 = (\xi_1)_1^2 + \dots + (\xi_{K_1})_1^2$  and  $\xi_2^2 = (\xi_1)_2^2 + \dots + (\xi_{K_2})_2^2$  and the internal degrees of freedom of  $\xi_1$  and  $\xi_2$  satisfy

$$K_1 + d = 2/(\gamma - 1), \quad K_2 + d = 6.$$

The parameters  $\lambda_1, \lambda_2$  can be given by

$$\frac{\rho}{2\lambda_1} = p, \quad \frac{\rho}{2\lambda_2} = \frac{1}{3} a_R T^4.$$

The collision term also satisfies the compatibility condition

$$\int \psi \frac{g - f}{\tau} d\Xi = 0,$$

where  $\psi = (1, u, v, \frac{1}{2}(u^2 + v^2 + \xi_1^2 + \xi_2^2))^T$  and  $d\Xi = du dv d\xi_1 d\xi_2$ .

According to the Chapman-Enskog expansion, the Euler and Navier-Stokes equations can be derived from the BGK equation [31, 32]. Similarly, the macroscopic equations Eq.(1) can be also

derived from Eq.(2). Taking zeroth-order Chapman-Enskog expansion, i.e. with  $f = g$ , and taking moments of BGK equation Eq.(2), we have

$$\int \psi(g_t + ug_x + vg_y) d\Xi = 0,$$

where

$$Q = \int \psi g d\Xi = \begin{pmatrix} \rho \\ \rho U \\ \rho V \\ \frac{1}{2}\rho(U^2 + V^2 + \frac{\rho U}{2\lambda_1} + \frac{\rho V}{2\lambda_2}) \end{pmatrix},$$

and

$$F(Q) = \int \psi ug d\Xi = \begin{pmatrix} \rho U^2 + \frac{\rho U}{2\lambda_1} + \frac{\rho}{2\lambda_2} \\ \frac{1}{2}\rho U(U^2 + V^2 + \frac{\rho U}{2\lambda_1} + \frac{\rho V}{2\lambda_2}) \end{pmatrix}.$$

According to the definition of  $\lambda_1, \lambda_2$  and the relation of  $K_1, K_2$ , the hyperbolic part of macroscopic equations Eq.(1) can be recovered and the vector form is used in the following sections

$$\frac{\partial Q}{\partial t} + \frac{\partial F(Q)}{\partial x} + \frac{\partial G(Q)}{\partial y} = S(Q),$$

where  $Q$  is the conservative variable,  $F(Q)$  and  $G(Q)$  are the fluxes in  $x$  and  $y$  directions and  $S(Q)$  is the source term for radiation diffusion.

### 3 High-order gas-kinetic scheme

#### 3.1 Temporal discretization

Recently, based on the time-dependent flux function of the generalized Riemann problem solver (GRP) [17,10] and gas-kinetic scheme (GKS) [22,13], a two-stage fourth-order time-accurate discretization was developed for Lax-Wendroff type flow solvers, particularly applied for the hyperbolic conservation laws. Considering the following time-dependent equation with the initial condition

$$\frac{dQ_{ij}}{dt} = \mathcal{L}(Q_{ij}),$$

where  $\mathcal{L}$  is an operator for spatial derivative of flux. Introducing an intermediate state at  $t^* = t_n + \Delta t/2$ , the two-stage temporal discretization can be written as

$$\begin{aligned} Q_{ij}^* &= Q_{ij}^n + \frac{1}{2}\Delta t \mathcal{L}(Q_{ij}^n) + \frac{1}{8}\Delta t^2 \frac{\partial}{\partial t} \mathcal{L}(Q_{ij}^n), \\ Q_{ij}^{n+1} &= Q_{ij}^n + \Delta t \mathcal{L}(Q_{ij}^n) + \frac{1}{6}\Delta t^2 \left( \frac{\partial}{\partial t} \mathcal{L}(Q_{ij}^n) + 2\frac{\partial}{\partial t} \mathcal{L}(Q_{ij}^*) \right). \end{aligned} \quad (3)$$

It can be proved that for the hyperbolic equations the two-stage time stepping method Eq.(3) provides a fourth-order time accurate solution for  $Q(t)$  at  $t = t_n + \Delta t$ . Based on the high-order spatial reconstruction [14,4], successes have also been achieved for the construction of high-order gas-kinetic scheme for Euler and Navier-Stokes equations [22,13]. The two-stage method provides a reliable framework to develop high-order scheme with the implementation of second-order flux function. Most importantly, due to the use of both flux function and its temporal derivative, this scheme is robust and works perfectly from the subsonic to the hypersonic flows.

In this paper, the high-order gas-kinetic scheme will be developed for the radiation hydrodynamics equation Eq.(1) as well. For simplicity, the two-dimensional uniform mesh is used. Taking moments of the BGK equation Eq.(2) and integrating with respect to space for the cell  $I_{ij} = [x_{i-1/2}, x_{i+1/2}] \times [y_{j-1/2}, y_{j+1/2}]$ , the semi-discrete finite volume scheme can be written as

$$\frac{dQ_{ij}}{dt} = \mathcal{L}(Q_{ij}) + \mathcal{S}(Q_{ij}), \quad (4)$$

where  $Q_{ij}$  is the cell averaged conservative variables over the cell  $I_{ij}$ . The operator  $\mathcal{L}(Q_{ij})$  for hydrodynamic part is given by

$$\mathcal{L}(Q_{ij}) = -\frac{1}{\Delta x}(F_{i+1/2,j}(t) - F_{i-1/2,j}(t)) - \frac{1}{\Delta y}(G_{i,j+1/2}(t) - G_{i,j-1/2}(t)), \quad (5)$$

and the operator  $\mathcal{S}(Q_{ij})$  is given by

$$\mathcal{S}(Q_{ij}) = \frac{1}{\Delta x \Delta y} S(Q_{ij}),$$

where  $\Delta x$  and  $\Delta y$  are the cell size,  $F_{i\pm 1/2,j}(t)$  and  $G_{i,j\pm 1/2}(t)$  are the time dependent numerical fluxes at cell interfaces in  $x$  and  $y$  directions and  $S(Q_{ij})$  is the source for radiation diffusion. Without considering the source term, the explicit scheme is used for the Euler and Navier-Stokes equations [22]. However, the time scales of radiation diffusion and fluid advection are different. It will make the time step of an explicit scheme very small, and the explicit scheme can be only used efficiently for the mildly non-relativistic regime for RHE. To improve the efficiency, the RHE should be discretized in an implicit-explicit (IMEX) procedure, i.e. the fluid advection term is treated explicitly and the radiation component is treated implicitly. Similar with Eq.(3), introducing an intermediate state  $Q^*$  at  $t^* = t_n + \Delta t/2$ , the two-stage temporal discretization for Eq.(4) is given as follows

$$\begin{aligned} Q_{ij}^* &= Q_{ij}^n + \frac{\Delta t}{2} \mathcal{L}(Q_{ij}^n) + \frac{\Delta t^2}{8} \mathcal{L}_t(Q_{ij}^n) + \frac{\Delta t}{4} (\mathcal{S}(Q_{ij}^n) + \mathcal{S}(Q_{ij}^*)), \\ Q_{ij}^{n+1} &= Q_{ij}^n + \Delta t \mathcal{L}(Q_{ij}^n) + \frac{\Delta t^2}{6} (\mathcal{L}_t(Q_{ij}^n) + 2\mathcal{L}_t(Q_{ij}^*)) + \frac{\Delta t}{6} (\mathcal{S}(Q_{ij}^n) + 4\mathcal{S}(Q_{ij}^*) + \mathcal{S}(Q_{ij}^{n+1})). \end{aligned} \quad (6)$$

Compared with the original two-stage method Eq.(3), the trapezoid integration is used for the source terms.

It can be proved that Eq.(6) provides a third-order accurate approximation for the system with sources Eq.(4) at  $t = t_n + \Delta t$ . Integrating Eq.(4) on the time interval  $[t^n, t^{n+1}]$ , we have

$$Q_{ij}^{n+1} - Q_{ij}^n = \int_{t_n}^{t_n + \Delta t} (\mathcal{L} + \mathcal{S})(Q_{ij}(t)) dt.$$

To prove this proposition above, the following Taylor expansion need to be satisfied

$$\begin{aligned} \int_{t_n}^{t_n + \Delta t} (\mathcal{L} + \mathcal{S})(Q_{ij}(t)) dt &= \Delta t (\mathcal{L} + \mathcal{S})(Q_{ij}^n) + \frac{\Delta t^2}{2} (\mathcal{L} + \mathcal{S})_t(Q_{ij}^n) \\ &\quad + \frac{\Delta t^3}{6} (\mathcal{L} + \mathcal{S})_{tt}(Q_{ij}^n) + \mathcal{O}(\Delta t^4). \end{aligned} \quad (7)$$

According to Eq.(4) and Cauchy-Kovalevskaya method, the temporal derivatives can be given by

$$\begin{aligned} \mathcal{L}_t &= \mathcal{L}_Q(\mathcal{L} + \mathcal{S}), \\ \mathcal{S}_t &= \mathcal{S}_Q(\mathcal{L} + \mathcal{S}), \end{aligned}$$

and

$$(\mathcal{L} + \mathcal{S})_{tt} = ((\mathcal{L}_Q Q + \mathcal{S}_Q Q)(\mathcal{L} + \mathcal{S})^2 + (\mathcal{L}_Q + \mathcal{S}_Q)^2(\mathcal{L} + \mathcal{S})).$$

For the operator  $\mathcal{S}$ , we have the following expansion up to the corresponding order

$$\begin{aligned}\mathcal{S}(Q_{ij}^*) &= \mathcal{S}(Q_{ij}^n) + \mathcal{S}_Q(Q_{ij}^* - Q_{ij}^n) + \frac{\mathcal{S}_{QQ}}{2}(Q_{ij}^* - Q_{ij}^n)^2 + \mathcal{O}(Q_{ij}^* - Q_{ij}^n)^3, \\ \mathcal{S}(Q_{ij}^{n+1}) &= \mathcal{S}(Q_{ij}^n) + \mathcal{S}_Q(Q_{ij}^{n+1} - Q_{ij}^n) + \frac{\mathcal{S}_{QQ}}{2}(Q_{ij}^{n+1} - Q_{ij}^n)^2 + \mathcal{O}(Q_{ij}^{n+1} - Q_{ij}^n)^3.\end{aligned}\quad (8)$$

Substituting Eq.(8) into Eq.(6), we have

$$\begin{aligned}Q_{ij}^* - Q_{ij}^n &= \frac{\Delta t}{2}(\mathcal{L}(Q_{ij}^n) + \mathcal{S}(Q_{ij}^n)) + \frac{\Delta t^2}{8}\mathcal{L}_t(Q_{ij}^n) + \frac{\Delta t}{4}\mathcal{S}_Q(Q_{ij}^* - Q_{ij}^n) + \mathcal{O}(\Delta t^3) \\ &= \frac{\Delta t}{2}(\mathcal{L}(Q_{ij}^n) + \mathcal{S}(Q_{ij}^n)) + \frac{\Delta t^2}{8}(\mathcal{L}_t(Q_{ij}^n) + \mathcal{S}_t(Q_{ij}^n)) + \mathcal{O}(\Delta t^3),\end{aligned}\quad (9)$$

and

$$\begin{aligned}Q_{ij}^{n+1} - Q_{ij}^n &= \Delta t(\mathcal{L}(Q_{ij}^n) + \mathcal{S}(Q_{ij}^n)) + \frac{\Delta t^2}{6}(\mathcal{L}_t(Q_{ij}^n) + 2\mathcal{L}_t(Q_{ij}^*)) \\ &\quad + \frac{\Delta t}{6}(\mathcal{S}_Q(Q_{ij}^{n+1} - Q_{ij}^n) + 4\mathcal{S}_Q(Q_{ij}^* - Q_{ij}^n)) \\ &\quad + \frac{\Delta t}{12}(\mathcal{S}_{QQ}(Q_{ij}^{n+1} - Q_{ij}^n)^2 + 4\mathcal{S}_{QQ}(Q_{ij}^* - Q_{ij}^n)^2).\end{aligned}\quad (10)$$

For the operator  $\mathcal{L}$ , we have the following expansion up to the corresponding order as well

$$\begin{aligned}\mathcal{L}(Q_{ij}^*) &= \mathcal{L}(Q_{ij}^n) + \mathcal{L}_Q(Q_{ij}^* - Q_{ij}^n) + \frac{\mathcal{L}_{QQ}}{2}(Q_{ij}^* - Q_{ij}^n)^2 + \mathcal{O}(Q_{ij}^* - Q_{ij}^n)^2, \\ \mathcal{L}_Q(Q_{ij}^*) &= \mathcal{L}_Q(Q_{ij}^n) + \mathcal{L}_{QQ}(Q_{ij}^* - Q_{ij}^n) + \frac{\mathcal{L}_{QQQ}}{2}(Q_{ij}^* - Q_{ij}^n)^2 + \mathcal{O}(Q_{ij}^* - Q_{ij}^n)^2.\end{aligned}\quad (11)$$

Substituting Eq.(9) and Eq.(11) into Eq.(10), it is easy to verify

$$\begin{aligned}Q_{ij}^{n+1} - Q_{ij}^n &= \Delta t(\mathcal{L} + \mathcal{S})(Q_{ij}^n) + \frac{\Delta t^2}{2}(\mathcal{L}_Q + \mathcal{S}_Q)(\mathcal{L} + \mathcal{S})(Q_{ij}^n) \\ &\quad + \frac{\Delta t^3}{6}((\mathcal{L}_{QQ} + \mathcal{S}_{QQ})(\mathcal{L} + \mathcal{S})^2 + (\mathcal{L}_Q + \mathcal{S}_Q)^2(\mathcal{L} + \mathcal{S}))(Q_{ij}^n) + \mathcal{O}(\Delta t^4).\end{aligned}$$

Therefore, the two-stage method Eq.(6) provides a third-order temporal discretization for radiation hydrodynamic equations.

### 3.2 Discretization for hydrodynamic part

In the following subsections, the implementation of the hydrodynamic part and radiative part will be given for Eq.(6). For the hydrodynamic part, the numerical flux  $F_{i+1/2,j}(t)$  in  $x$ -direction can be given by Gaussian quadrature

$$F_{i+1/2,j}(t) = \frac{1}{\Delta y} \int_{y_{j-1/2}}^{y_{j+1/2}} F_{i+1/2}(y, t) dy = \sum_{\ell=1}^2 \omega_{\ell} \int \psi u f(x_{i+1/2}, y_{j\ell}, t, u, v, \xi) d\Xi, \quad (12)$$

where  $(x_{i+1/2}, y_{j\ell})$  is the Gaussian quadrature point and  $\omega_{\ell}$  are quadrature weights. To construct the gas distribution function  $f(x_{i+1/2}, y_{j\ell}, t, u, v, \xi)$  at the cell interface, the integral solution of BGK equation Eq.(2) is used

$$f(x_{i+1/2}, y_{j\ell}, t, u, v, \xi) = \frac{1}{\tau} \int_0^t g(x', y', t', u, v, \xi) e^{-(t-t')/\tau} dt' + e^{-t/\tau} f_0(-ut, -vt, u, v, \xi), \quad (13)$$

where  $f_0$  is the initial gas distribution function,  $g$  is the corresponding equilibrium state, and  $x_{i+1/2} = x' + u(t - t')$  and  $y_{j\ell} = y' + v(t - t')$  are the trajectory of particles. Similar with the

gas-kinetic scheme for Euler and Navier-Stokes equations, the second-order gas-kinetic solver [32] can be written as follows

$$\begin{aligned} f(x_{i+1/2}, y_{je}, t, u, v, \xi) = & (1 - e^{-t/\tau})g_0 + ((t + \tau)e^{-t/\tau} - \tau)(\bar{a}u + \bar{b}v)g_0 \\ & + (t - \tau + \tau e^{-t/\tau})\bar{A}g_0 \\ & + e^{-t/\tau}g_r[1 - (\tau + t)(a^ru + b^rv) - \tau A^r](1 - H(u)) \\ & + e^{-t/\tau}g_l[1 - (\tau + t)(a^lu + b^lv) - \tau A^l]H(u). \end{aligned} \quad (14)$$

The coefficients in Eq.(14) can be determined by the reconstructed derivatives and compatibility condition

$$\langle a^{l,r} \rangle = \frac{\partial Q_{l,r}}{\partial x}, \langle b^{l,r} \rangle = \frac{\partial Q_{l,r}}{\partial y}, \langle a^{l,r}u + b^{l,r}v + A^{l,r} \rangle = 0,$$

and

$$\langle \bar{a} \rangle = \frac{\partial Q_0}{\partial x}, \langle \bar{b} \rangle = \frac{\partial Q_0}{\partial y}, \langle \bar{a}u + \bar{b}v + \bar{A} \rangle = 0,$$

where the moments of the equilibrium  $g$  are defined by

$$\langle \dots \rangle = \int g(\dots) \psi d\Xi.$$

Compared with the Euler and Navier-Stokes equations, the procedure for RHE is a little more complicated. As an example, the spatial derivative of  $g$  can be written as

$$\frac{\partial g}{\partial x} = ag, \quad (15)$$

where

$$a = \mathbf{a} \cdot \tilde{\psi} = a_1 + a_2u + a_3v + \frac{1}{2}a_4(u^2 + v^2) + \frac{1}{2}a_5\xi_1^2 + \frac{1}{2}a_6\xi_2^2.$$

Taking moments of Eq.(15), we have

$$\frac{\partial Q}{\partial x} = \int \frac{\partial g}{\partial x} \psi d\Xi = \int ag\psi d\Xi,$$

To obtain the connections  $\mathbf{a} = (a_1, \dots, a_6)$ , the equation can be given as a linear system

$$M\mathbf{a} = \frac{\partial Q}{\partial x}, \quad (16)$$

where

$$M = \int \psi \otimes \tilde{\psi} g d\Xi.$$

The detailed formulation of  $M$  can be found in Appendix. The system Eq.(16) seems to be under determined, but we can also find the unique solution.

According to the chain rule, the derivative of  $g$  can be also written as

$$\frac{\partial g}{\partial x} = \frac{\partial g}{\partial \rho} \frac{\partial \rho}{\partial x} + \frac{\partial g}{\partial U} \frac{\partial U}{\partial x} + \frac{\partial g}{\partial V} \frac{\partial V}{\partial x} + \frac{\partial g}{\partial \lambda_1} \frac{\partial \lambda_1}{\partial x} + \frac{\partial g}{\partial \lambda_2} \frac{\partial \lambda_2}{\partial x}.$$

It's easily to verify that

$$\frac{\partial g}{\partial \lambda_1} = C_1g - \xi_1^2g, \quad \frac{\partial g}{\partial \lambda_2} = C_2g - \xi_2^2g,$$

where  $C_1$  and  $C_2$  are the functions without  $\xi_1^2$  and  $\xi_2^2$ , respectively. Comparing the coefficients of  $\xi_1^2$  and  $\xi_2^2$  with Eq.(15), we have

$$\frac{1}{2}a_5\xi_1^2g = -\xi_1^2g \frac{\partial \lambda_1}{\partial x}, \quad \frac{1}{2}a_6\xi_2^2g = -\xi_2^2g \frac{\partial \lambda_2}{\partial x}.$$



According to the definition of  $\lambda_1$  and  $\lambda_2$ , we have

$$\begin{aligned} a_5 &= -2 \frac{\partial \lambda_1}{\partial x} = \frac{T_x}{RT^2}, \\ a_6 &= -2 \frac{\partial \lambda_2}{\partial x} = -\frac{\rho_x T - 4\rho T_x}{a_R T^5/3}, \end{aligned}$$

where

$$T_x = \frac{1}{\rho c_v + 4a_R T^3} \left( (E_x^* - \frac{(\rho U)(\rho U)_x + (\rho V)(\rho V)_x}{\rho}) + \frac{((\rho U)^2 + (\rho V)^2)\rho_x}{2\rho^2} - \rho_x c_v T \right).$$

With the solution for  $a_5$  and  $a_6$ , the unique solution of the linear system is given by

$$\begin{aligned} a_4 &= \left( \frac{1}{\rho} (A - UB - VC) - \frac{K_1}{8\lambda_1^2} a_5 - \frac{K_2}{8\lambda_2^2} a_6 \right) / L^2, \\ a_3 &= \frac{1}{\rho L} C - V a_4, \\ a_2 &= \frac{1}{\rho L} B - U a_4, \\ a_1 &= \frac{1}{\rho} \frac{\partial \rho}{\partial x} - U a_2 - V a_3 - B'_1 a_4 - \frac{K_1}{4\lambda_1} a_5 - \frac{K_2}{4\lambda_2} a_6, \end{aligned}$$

where

$$\begin{aligned} A &= \frac{\partial E^*}{\partial x} - \frac{1}{2} (U^2 + V^2 + \frac{K_1 + 2}{2\lambda_1} + \frac{K_2 + 2}{2\lambda_2}) \frac{\partial \rho}{\partial x}, \\ B &= \frac{\partial(\rho U)}{\partial x} - U \frac{\partial \rho}{\partial x}, \\ C &= \frac{\partial(\rho V)}{\partial x} - V \frac{\partial \rho}{\partial x}, \\ L &= \frac{1}{2\lambda_1} + \frac{1}{2\lambda_2}. \end{aligned}$$

Similarly, the coefficients for temporal derivative can be also determined. Thus, the gas distribution function Eq.(14) and the numerical fluxes  $F_{i+1/2,j}(Q^n, t)$  Eq.(12) can be fully constructed.

In order to utilize the two-stage temporal discretization, the temporal derivatives of the flux function need to be determined. The flux  $F_{i+1/2,j}(Q^n, t)$  in the time interval  $[t_n, t_n + \Delta t]$  is expanded as the following linear form

$$F_{i+1/2,j}(t) = F_{i+1/2,j}^n + \partial_t F_{i+1/2,j}^n (t - t_n). \quad (17)$$

where the coefficients  $F_{i+1/2,j}^n$  and  $\partial_t F_{i+1/2,j}^n$  can be fully determined by solving the linear system

$$\begin{aligned} F_{i+1/2,j}^n \Delta t + \frac{1}{2} \partial_t F_{i+1/2,j}^n \Delta t^2 &= \int_{t_n}^{t_n + \Delta t} F_{i+1/2,j}(t) dt, \\ \frac{1}{2} F_{i+1/2,j}^n \Delta t + \frac{1}{8} \partial_t F_{i+1/2,j}^n \Delta t^2 &= \int_{t_n}^{t_n + \Delta t/2} F_{i+1/2,j}(t) dt. \end{aligned}$$

Similarly, the coefficients  $G_{i,j+1/2}^n$  and  $\partial_t G_{i,j+1/2}^n$  corresponding to the flux  $G_{i,j+1/2}(t)$  in  $y$ -direction can be constructed as well. According to Eq.(5),  $\mathcal{L}(Q_{ij}^n)$  and its temporal derivative  $\partial_t \mathcal{L}(Q_{ij}^n)$  at  $t^n$  can be given by

$$\begin{aligned} \mathcal{L}(Q_{ij}^n) &= -\frac{1}{\Delta x} (F_{i+1/2,j}^n(t) - F_{i-1/2,j}^n(t)) - \frac{1}{\Delta y} (G_{i,j+1/2}^n(t) - G_{i,j-1/2}^n(t)), \\ \partial_t \mathcal{L}(Q_{ij}^n) &= -\frac{1}{\Delta x} (\partial_t F_{i+1/2,j}^n(t) - \partial_t F_{i-1/2,j}^n(t)) - \frac{1}{\Delta y} (\partial_t G_{i,j+1/2}^n(t) - \partial_t G_{i,j-1/2}^n(t)). \end{aligned}$$

With the procedure at the intermediate state,  $\mathcal{L}(Q_{ij}^*)$ ,  $\partial_t \mathcal{L}(Q_{ij}^*)$  can be constructed as well.

### 3.3 Discretization for radiative part

According to the definition of source terms, we only need to solve energy equations at two-stages for Eq.(6), which are nonlinear systems with respect to the temperature  $T$ . At each stage, the energy equations can be simplified as the nonlinear system

$$\mathcal{F}(T) = 0, \quad (18)$$

where  $\mathcal{F}$  is a nonlinear function from  $R^N$  to  $R^N$  and  $N$  is the number of cells. To obtain an approximate solution of the nonlinear system, the above system is rewritten as

$$\mathcal{J}\delta = -\mathcal{F},$$

where  $\mathcal{J}$  is the Jacobian of  $\mathcal{F}$ . In order to avoid calculating the Jacobian directly,  $\mathcal{J}$  can be approximated by the  $F$ -derivative as follows

$$\mathcal{J}(T) \cdot \delta = \frac{\mathcal{F}(T + \sigma\delta) - \mathcal{F}(T)}{\sigma}, \quad (19)$$

where  $\sigma$  is a small scalar. In fact, it is not trivial to choose  $\sigma$ , which has great influence on the stability of algorithm and improper values will cause blowing up. According to [5], a special  $\sigma$  is given as follows

$$\sigma = \frac{\sqrt{\eta}}{\|\delta\|_2^2} \max\{|T \cdot \delta|, \text{typ}T \cdot |\delta|\} \cdot \text{sign}(T \cdot \delta),$$

where  $\eta$  is the machine epsilon,  $|\delta| = (|\delta_1|, \dots, |\delta_N|)^T$ ,  $\text{typ}T = (\text{typ}T_1, \dots, \text{typ}T_N)^T$ ,  $\text{typ}T_i$  is the typical size of  $T_i$  and the typical size of real number equals to its order of magnitude plus one. With the initial guess  $T^{(0)}$  for Eq.(18) and  $\delta^{(0)}$  for Eq.(19), the initial residual is

$$r^{(0)} = -\mathcal{F} - \mathcal{J}\delta^{(0)},$$

and its generated Krylov subspace is

$$K_m \equiv \text{span}\{r^{(0)}, \mathcal{J}r^{(0)}, \dots, \mathcal{J}^{m-1}r^{(0)}\}.$$

According to the nonlinear Newton-GMRES method [5], an approximate solution can be given. Besides, in order to improve computation efficiency, a restart algorithm is applied in orthogonalization process [24]. In actual calculation, the restart times can be no more than 5 times if the restart step and convergence condition are set appropriately.

## 4 Numerical tests

In this section, the one and two dimensional tests cases are provided to the correctness and robustness of current scheme. In the computation, the collision time  $\tau$  takes

$$\tau = \epsilon\Delta t + C \left| \frac{p_l - p_r}{p_l + p_r} \right| \Delta t,$$

where  $p_l$  and  $p_r$  denote the pressure on the left and right sides of the cell interface. In smooth flow regions, the collision term takes  $\tau = 0$  and the gas distribution function Eq.(14) will reduce to

$$f = g_0(1 + \bar{A}t).$$

To achieve the spatial accuracy, the classical multidimensional fifth-order WENO reconstruction is adopted and more details can be found in [22, 4]. In order to eliminate the spurious oscillation and improve the stability, the WENO reconstruction is performed for the characteristic variables, and the detailed analysis for characteristics can be found in [8]. Without special statement, the gas with  $\gamma = 5/3$  is used in the following numerical examples.

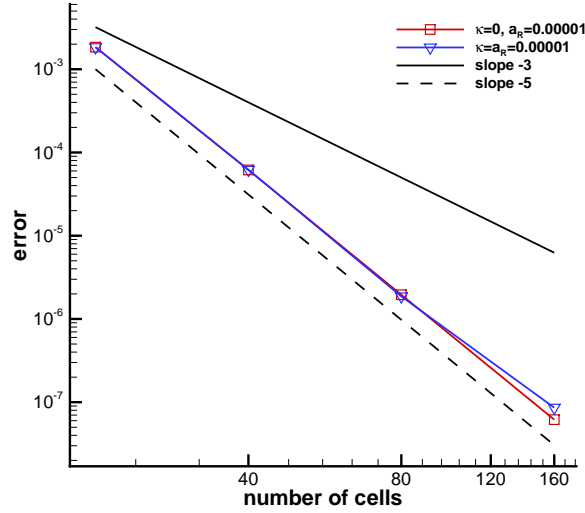
num of cells	$L^1$ error	Order	$L^2$ error	Order
10	1.9001E-03		1.5274E-03	
20	6.3660E-05	4.8995	5.0075E-05	4.9307
40	2.0139E-06	4.9822	1.5793E-06	4.9867
80	6.3035E-08	4.9977	4.9421E-08	4.9980
160	1.9698E-09	5.0000	1.5443E-09	5.0001

**Table 1** Accuracy test: errors and orders of accuracy with  $\kappa = 0$  and  $a_R = 0$  at  $t = 2$ .

num of cells	$L^1$ error	$L^2$ error
20	1.8422E-03	1.4787E-03
40	6.1674E-05	4.8513E-05
80	1.9536E-06	1.5314E-06
160	6.1704E-08	4.8354E-08

**Table 2** Accuracy test: errors of  $\|U_N - U_{N/2}\|$  with  $\kappa = 0$  and  $a_R = 10^{-5}$  at  $t = 2$ .

num of cells	$L^1$ error	$L^2$ error
20	1.8407E-03	1.4782E-03
40	6.1984E-05	4.8438E-05
80	1.8685E-06	1.4935E-06
160	8.5963E-08	7.5867E-08

**Table 3** Accuracy test: errors of  $\|U_N - U_{N/2}\|$  with  $\kappa = 10^{-5}$  and  $a_R = 10^{-5}$  at  $t = 2$ .**Fig. 1** Accuracy test: log-log plots for  $L^1$  and  $L^2$  norms of  $\|U_N - U_{N/2}\|$  and number of cells  $N$  at  $t = 2$ .

#### 4.1 Accuracy test

The advection of density perturbation problem for Euler equations is extended to test the order of accuracy for RHE. In this test case, the initial condition is set as follows

$$\rho(x) = 1 + 0.2 \sin(\pi x), \quad u(x) = 1, \quad p(x) = 1,$$

where the computational domain is  $[0, 2]$ , the periodic boundary condition is applied and  $c_v = 1/(\gamma - 1)$ .

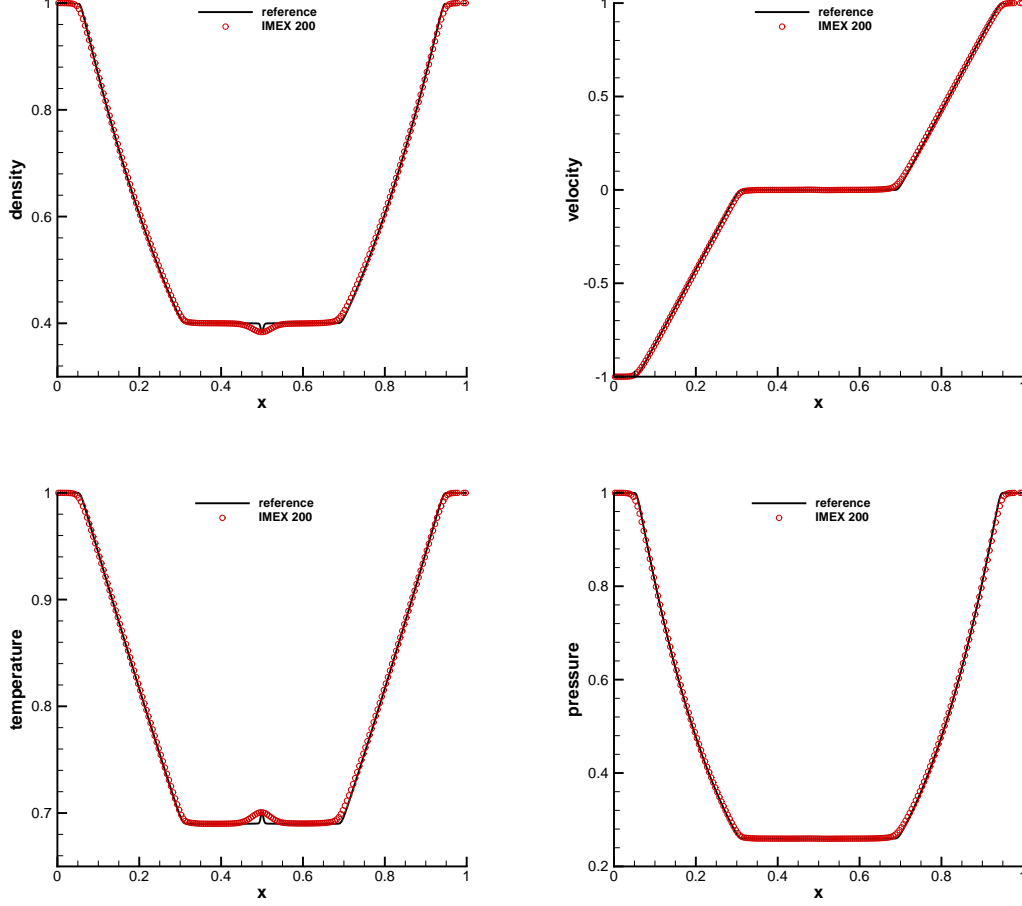


**Fig. 2** Shock tube problem involving two rarefactions for density, velocity, temperature and pressure at  $t = 0.2$  with  $\kappa = 0$  for the numerical results and reference data.

As reference, the case with  $\kappa = 0$  and  $a_R = 0$  is tested. With these parameters, the RHE degenerates into the Euler equation and the exact solution can be given by

$$\rho(x, t) = 1 + 0.2 \sin(\pi(x - t)), \quad u(x, t) = 1, \quad p(x, t) = 1.$$

The  $L^1$  and  $L^2$  errors and orders at  $t = 2$  are shown in Table.1 with uniform meshes, where  $\Delta x = 2/N$  and  $N$  is the number of cells. The expected order of accuracy can be achieved. To test the accuracy with radiative effect, two cases with  $\kappa = 0, a_R = 10^{-5}$  and  $\kappa = 10^{-5}, a_R = 10^{-5}$  are tested. In the computation, the periodic boundary condition is also imposed, and the uniform meshes with  $N$  cells are used. For these two cases, they have no exact solution, and  $\|U_N - U_{N/2}\|$  is computed, where the nonlinear source term is discretized by a high-order central difference. For the case with  $\kappa = 0$ , the system is hyperbolic and the GMRES process is not needed. It falls into the classical two-stage fourth-order method Eq.(3). For the case with non-zero  $\kappa$ , the GMRES process is needed and the tolerance for convergence is set as  $10^{-9}$ . The  $L^1$  and  $L^2$  norms of  $\|U_N - U_{N/2}\|$  at  $t = 2$  are given in Table.2 and Table.3. The log-log plots for  $L^1$  and  $L^2$  norms of  $\|U_N - U_{N/2}\|$  and number of cells  $N$  is given in Fig.1. With the influence of radiation effect and nonlinear source, the theoretical order of accuracy can be well kept with the mesh refinement.

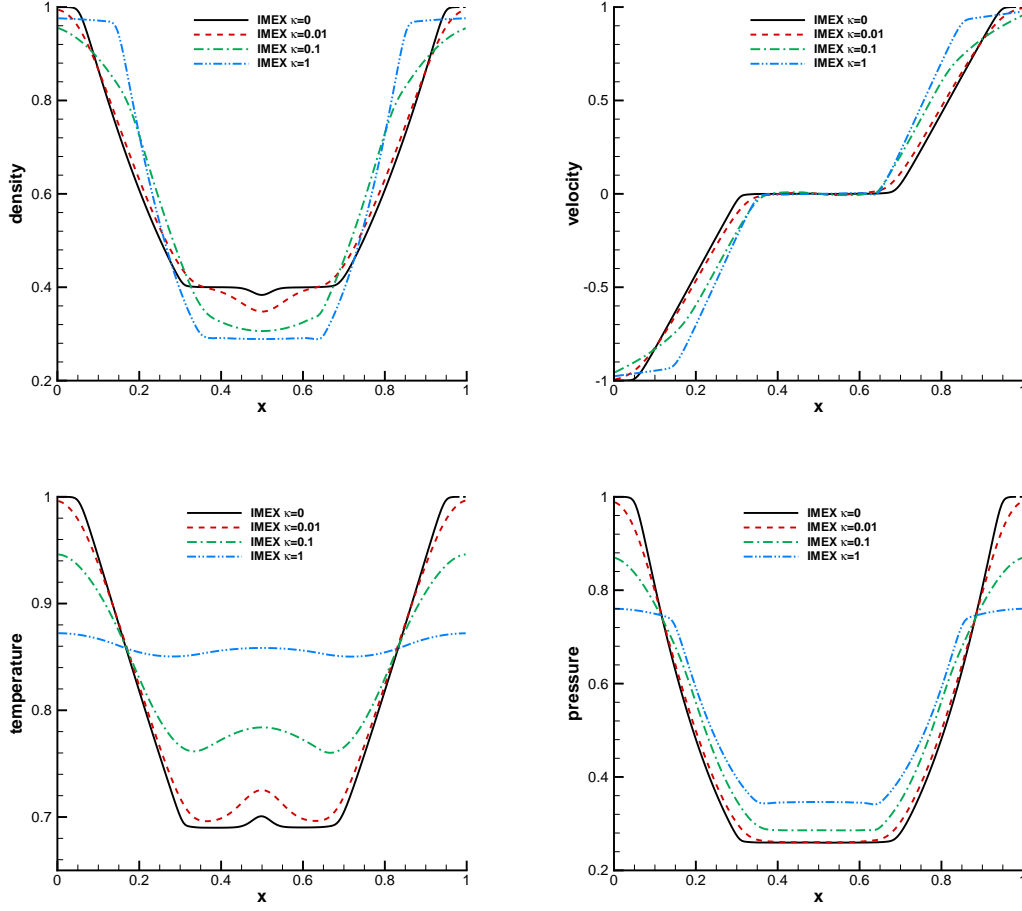


**Fig. 3** Shock tube problem involving two rarefactions: density, velocity, temperature and pressure at  $t = 0.2$  with  $\kappa = 0, 0.01, 0.1$  and  $1$ .

#### 4.2 Shock tube problem with two rarefaction waves

In this case, this one-dimensional shock tube problem is tested, which involves two rarefaction waves moving towards the opposite directions. The computational domain is  $[-0.5, 0.5]$ , and the following initial condition is considered

$$(\rho, U, T) = \begin{cases} (1, -1, 1), & 0 \leq x < 0.5, \\ (1, 1, 1), & 0.5 \leq x \leq 1, \end{cases}$$

where  $c_v = 1$  and  $a_R = 1$ . For the system without the diffusion term, i.e.,  $\kappa = 0$ , the uniform mesh with 200 cells is used. The numerical results and the reference solutions are given in Fig.2, where the reference solutions are given by the second-order code with 2000 cells. The numerical results also agree well with the reference solutions [8]. To test the effect of the radiative diffusion, the cases with  $\kappa = 1, 0.01$  and  $0.1$  are tested as well. The numerical results are shown in Fig.3, and the numerical results agree well with [8]. With the increase of  $\kappa$ , the results reveal that the diffusion effect becomes more obvious, and such phenomena is quite reasonable in physics.

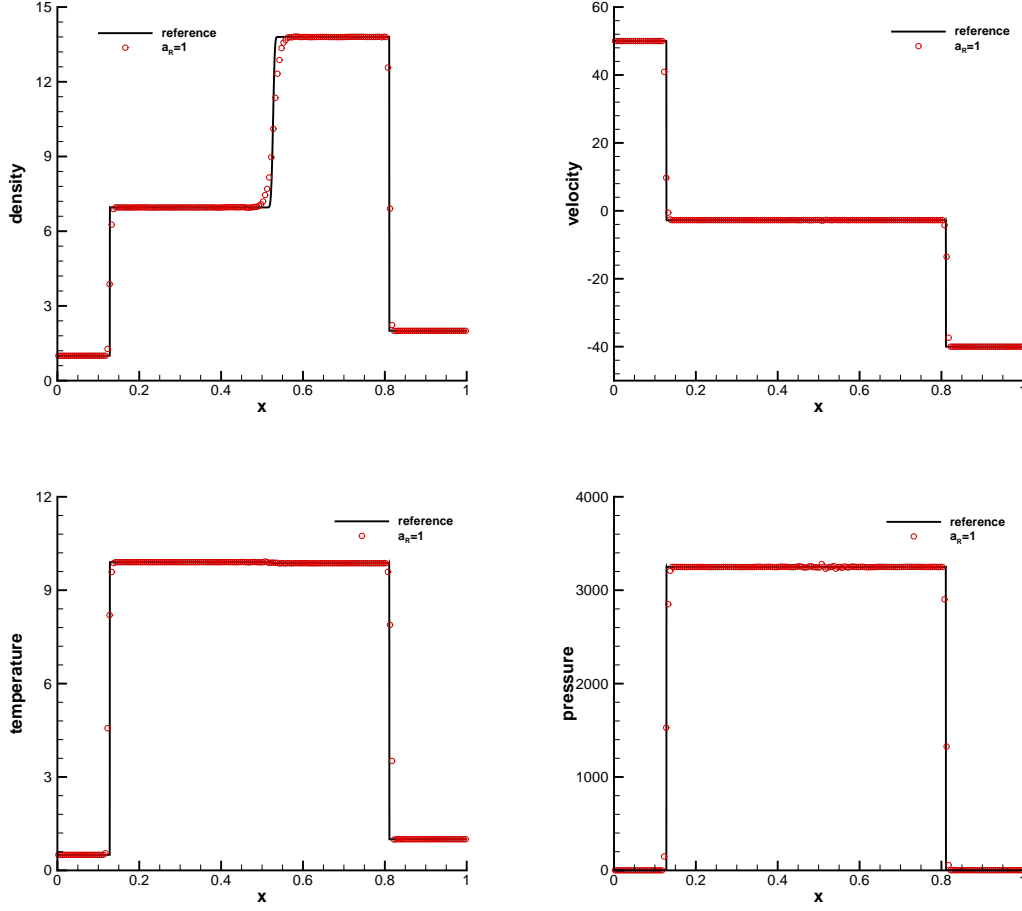


**Fig. 4** Shock tube problem involving two shock waves: density, velocity, temperature and pressure at  $t = 0.045$  with  $a_R = 1$  for the numerical results and reference data.

#### 4.3 Shock tube problem with two shock waves

In this case, the one-dimensional shock tube problem involving two strong shock waves is tested. The computational domain is  $[0, 1]$ , and the following initial condition is considered

$$(\rho, U, T) = \begin{cases} (1, 50, 0.5), & 0 \leq x \leq 0.65, \\ (2, -40, 1), & 0.65 \leq x \leq 1, \end{cases}$$

where  $c_v = 1$ ,  $a_R = 1$  and  $\kappa = 0$ . Two shocks with Mach numbers about 82 and 39 are generated from the initial discontinuity. The uniform mesh with 200 cells are used. The numerical results and reference solutions at  $t = 0.045$  are given in Fig.5, where the reference solutions are given by the second-order code with 10000 cells. For this case, the exact solutions for  $(\rho, U, T)$  at two sides of contact discontinuity are  $(6.95456, 9.90081, -2.73959)$  and  $(13.8008, 9.86595, -2.73959)$  according to the nonlinear Riemann solver [9]. The numerical solutions are in a good agreement with the exact solutions. The radiation effect  $a_R$  is tested as well, where  $a_R = 0.0001, 0.01, 0.1$  and  $1$  are used, and the numerical results are shown in Fig.4. Due to the strong discontinuity, there is slight oscillation across the contact discontinuity even with the reconstruction for characteristic variables [3].

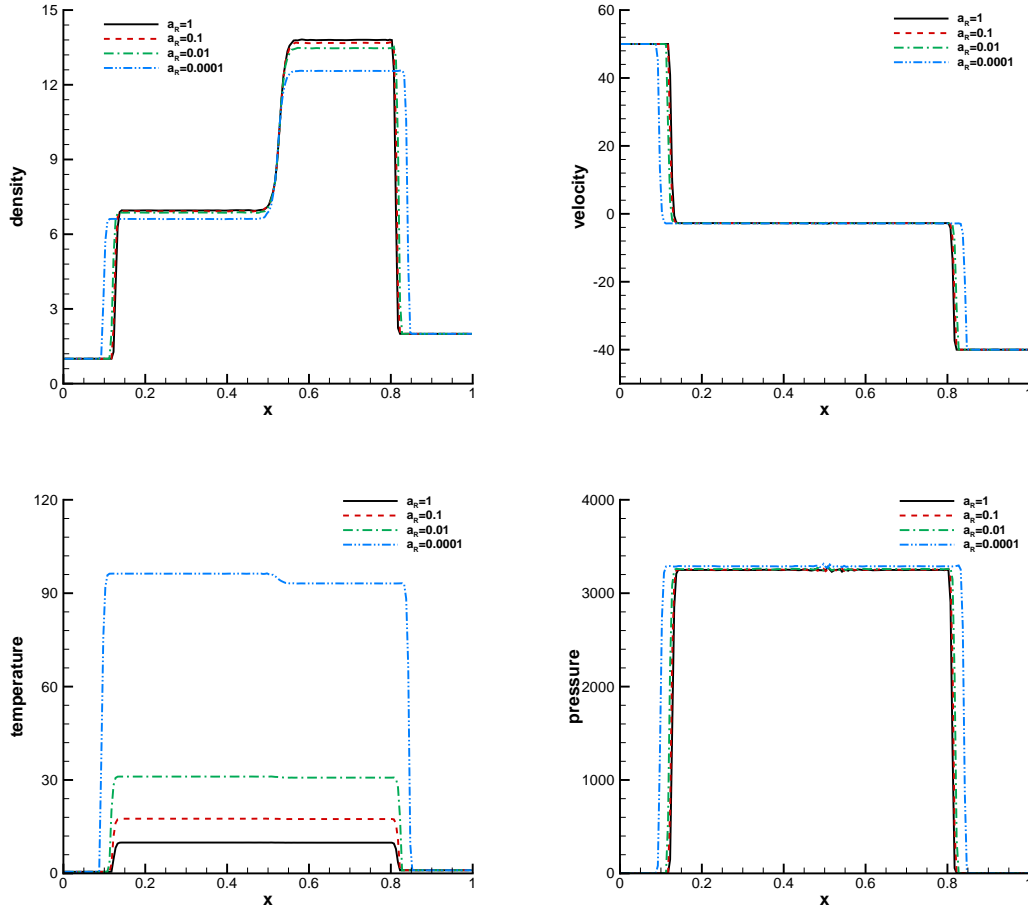


**Fig. 5** Shock tube problem involving two shock waves: density, velocity, temperature and pressure at  $t = 0.045$  with  $a_R = 0.0001, 0.01, 0.1$  and  $1$ .

#### 4.4 Interaction between wind and cylindrical bubble

In this case, the two-dimensional interactions between wind and denser cylindrical bubble are tested. The simulation is performed in the domain  $[0, 2] \times [0, 1]$ , and there is a cylindrical bubble of radius  $R = 0.15$  with its center located at  $(0.3, 0.5)$ . The bubble is 25 times denser than the ambient gas, and the temperature of the cloud is such that the cloud and ambient gas are in an equilibrium state. Initially, the state for the ambient gas is  $(\rho, U, V, T) = (1, 0, 0, 0.09)$ , and the wind is introduced through the left boundary and assigned as

$$(\rho, U, V, T) = (1, 6(1 - e^{-10t}), 0, 0.09).$$

The zero gradient boundary condition is given at the right, upper and lower boundaries and  $a_R$  is taken to be 1. The computation is performed with  $240 \times 120$  uniform mesh. For the case with  $\kappa = 0$ , the density, pressure and temperature distributions at  $t = 0.6$  are shown in Fig.6, where the simulated results reproduce the large-scale structure of the reference results, and the high-order scheme resolves the flow structures better than the second order scheme [30,15]. The case with heat diffusivity  $\kappa(T) = 10^{-3}(1 + 10T^3)$  is also tested. The density, pressure and temperature distributions at  $t = 0.6$  are shown in Fig.7. Due to the heat diffusivity, the flow structures are smeared.

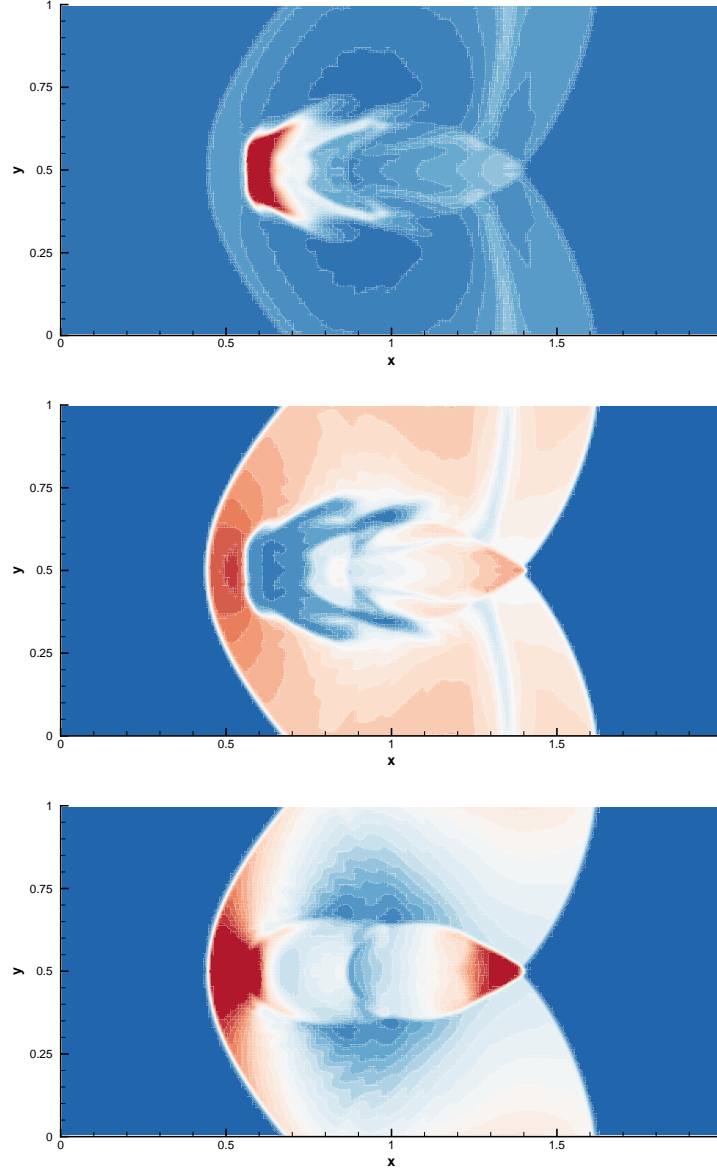


**Fig. 6** Wind and cylindrical bubble interaction: the density, pressure and temperature distributions at  $t = 0.6$  from top to bottom with  $\kappa(T) = 0$ .

#### 4.5 Computational efficiency

In this case, the computational efficiency of shock tube problem and interaction between wind and bubble are tested for both one-dimensional and two-dimensional computation. To show the efficiency of GMRES procedure, the case with and without heat diffusivity are tested, respectively. In the computation, the dimension of Krylov subspace in restart procedure is 10, and the convergence tolerance of GMRES method is  $10^{-8}$ . The CPU times for different cases are shown in Table.4 with Intel Core i7-9700 CPU @ 3.00 GHz within 400 time steps. The comparison of CPU time shows the efficiency of implicit-explicit high-order gas-kinetic scheme with GRMES procedure.



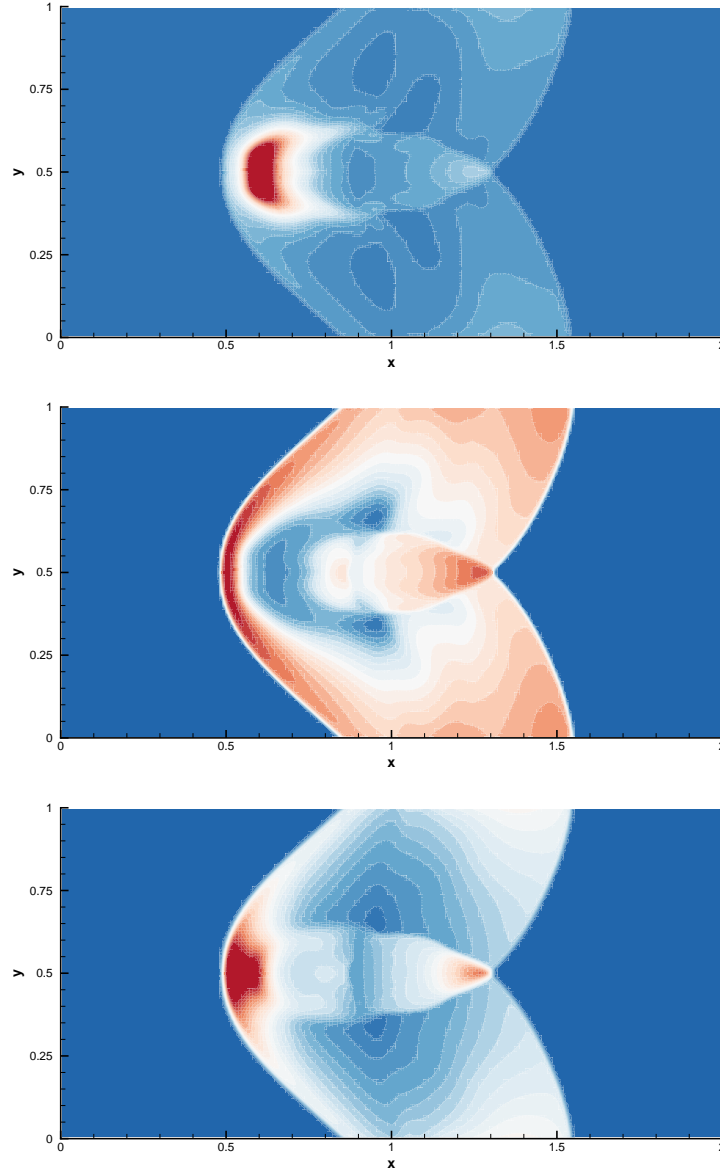


**Fig. 7** Wind and cylindrical bubble interaction: the density, pressure and temperature distributions at  $t = 0.6$  from top to bottom with  $\kappa(T) = 10^{-3}(1 + 10T^3)$ .

	$\kappa$	CPU time
1D case	$\kappa = 0$	2.725
1D case	$\kappa = 0.01$	3.507
2D case	$\kappa = 0$	81.063
2D case	$\kappa = 10^{-3}(1 + 10T^3)$	266.956

**Table 4** Computational efficiency: CPU time (seconds) comparison.

## 5 Conclusion

In this paper, a high-order gas-kinetic scheme is proposed for the equation of radiation hydrodynamic in the equilibrium-diffusion limit. Based on the zeroth-order Chapman-Enskog expansion, the hydrodynamic part of radiation hydrodynamic equation can be obtained from the modified

BGK equation with modified equilibrium state. The numerical scheme is developed in the finite volume framework, and the classical multidimensional WENO reconstruction is used to achieve the spatial accuracy. To achieve the temporal accuracy, a two-stage method is used, which is an extension of two-stage fourth-order method for hyperbolic system. The time scales of radiation diffusion and hydrodynamic part are different and it will make the time step of an explicit scheme very small, and an IMEX-type scheme is developed. The hydrodynamic part is treated explicitly, and the gas-kinetic solver with the modified equilibrium state is constructed in the finite volume framework. The nonlinear Newton-GMRES method is used to treat the radiation diffusion implicitly, in which the formation of Jacobian is not required. One-dimensional and two-dimensional numerical experiments are carried out, and the numerical results validate the performance of current scheme.

## Acknowledgements

The current research of L. Pan is supported by National Natural Science Foundation of China (11701038) and the Fundamental Research Funds for the Central Universities, and W.J. Sun is supported by CAEP foundation (CX20200026) and National Natural Science Foundation of China (11671048).

## Appendix

The detailed formulation of matrix  $M$  in Eq.(16) can be written as

$$M = \begin{pmatrix} 1 & U & V & B'_1 & \frac{K_1}{4\lambda_1} & \frac{K_2}{4\lambda_2} \\ U & U^2 + \frac{1}{2\lambda_1} + \frac{1}{2\lambda_2} & UV & B'_2 & \frac{K_1}{4\lambda_1}U & \frac{K_2}{4\lambda_2}U \\ V & UV & V^2 + \frac{1}{2\lambda_1} + \frac{1}{2\lambda_2} & B'_3 & \frac{K_1}{4\lambda_1}V & \frac{K_2}{4\lambda_2}V \\ B_1 & B_2 & B_3 & B_4 & B_5 & B_6 \end{pmatrix},$$

where

$$\begin{aligned} B_1 &= \frac{1}{2}(U^2 + V^2 + \frac{K_1+2}{2\lambda_1} + \frac{K_2+2}{2\lambda_2}), & B'_1 &= \frac{1}{2}(U^2 + V^2 + \frac{1}{\lambda_1} + \frac{1}{\lambda_2}), \\ B_2 &= \frac{1}{2}U(U^2 + V^2 + \frac{K_1+4}{2\lambda_1} + \frac{K_2+4}{2\lambda_2}), & B'_2 &= \frac{1}{2}U(U^2 + V^2 + \frac{2}{\lambda_1} + \frac{2}{\lambda_2}), \\ B_3 &= \frac{1}{2}V(U^2 + V^2 + \frac{K_1+4}{2\lambda_1} + \frac{K_2+4}{2\lambda_2}), & B'_3 &= \frac{1}{2}V(U^2 + V^2 + \frac{2}{\lambda_1} + \frac{2}{\lambda_2}), \\ B_4 &= \frac{1}{4}((U^2 + V^2 + \frac{1}{\lambda_1} + \frac{1}{\lambda_2})(U^2 + V^2 + \frac{K_1+2}{2\lambda_1} + \frac{K_2+2}{2\lambda_2}) \\ &\quad + (\frac{2}{\lambda_1} + \frac{2}{\lambda_2})(U^2 + V^2 + \frac{1}{2\lambda_1} + \frac{1}{2\lambda_2})), \\ B_5 &= \frac{1}{4}(\frac{K_1}{2\lambda_1}(U^2 + V^2) + \frac{K_1^2 + 4K_1}{4\lambda_1^2} + \frac{K_1(K_2+2)}{4\lambda_1\lambda_2}), \\ B_6 &= \frac{1}{4}(\frac{K_2}{2\lambda_2}(U^2 + V^2) + \frac{K_2^2 + 4K_2}{4\lambda_2^2} + \frac{K_2(K_1+2)}{4\lambda_1\lambda_2}). \end{aligned}$$

## References

1. J.W. Bates, D.A. Knoll, W.J. Rider, R.B. Lowrie, V.A. Mousseau, On consistent time-integration methods for radiation hydrodynamics in the equilibrium diffusion limit: Low-energy-density regime, J. Comput. Phys. 167 (2001) 99-130.
2. P.L. Bhatnagar, E.P. Gross, M. Krook, A Model for Collision Processes in Gases I: Small Amplitude Processes in Charged and Neutral One-Component Systems, Phys. Rev. 94 (1954) 511-525.

3. S. Bolding, J. Hansel, J.D. Edwards, J.E. Morel, R.B. Lowrie, Second-order discretization in space and time for radiation-hydrodynamics, *J. Comput. Phys.* 338 (2017) 511-526.
4. R. Borges, M. Carmona, B. Costa, W. S. Don, An improved weighted essentially non-oscillatory scheme for hyperbolic conservation laws, *J. Comput. Phys.* 227 (2008) 3191-3211.
5. P. N. Brown, Y. Saad, Hybrid Krylov Methods for Nonlinear Systems of Equations, *SIAM J. Sci. Comput.* 11 (1990) 450-481.
6. J.I. Castor, *Radiation Hydrodynamics*, Cambridge University Press (2004).
7. S. Chapman, T.G. Cowling, *The Mathematical theory of Non-Uniform Gases*, third edition, Cambridge University Press, (1990).
8. J. Cheng, C.W. Shu, P. Song, High order conservative Lagrangian schemes for one-dimensional radiation hydrodynamics equations in the equilibrium-diffusion limit, *J. Comput. Phys.* 421 (2020) 109724.
9. W. Dai, P.R. Woodward, Numerical simulations for radiation hydrodynamics. I. Diffusion limit, *J. Comput. Phys.* 142 (1998) 182-207.
10. Z.F. Du, J.Q. Li, A Hermite WENO reconstruction for fourth order temporal accurate schemes based on the GRP solver for hyperbolic conservation laws, *J. Comput. Phys.* 355 (2018) 385-396.
11. A. Harten, B. Engquist, S. Osher, S.R. Chakravarthy, Uniformly high order accurate essentially non-oscillatory schemes, III, *J. Comput. Phys.* 71 (1987) 231-303.
12. J. Huang, K. Xu, P. Yu, A unified gas-kinetic scheme for continuum and rarefied flows II: multi-dimensional cases, *Commun. Comput. Phys.* 12 (2012) 662-690.
13. X. Ji, L. Pan, W. Shyy, K. Xu, A compact fourth-order gas-kinetic scheme for the Euler and Navier-Stokes equations, *J. Comput. Phys.* 372 (2018) 446-472.
14. G.S. Jiang, C.W. Shu, Efficient implementation of weighted ENO schemes, *J. Comput. Phys.* 126 (1996) 202-228.
15. S. Jiang, W.J. Sun, A second-order BGK scheme for the equations of radiation hydrodynamics, *Int. J. Numer. Meth. Fluids* 53 (2007) 391-416.
16. D.A. Knoll, R.B. Lowrie, J.E Morel, Numerical analysis of time integration errors for non equilibrium radiation diffusion, *J. Comput. Phys.* 226 (2007) 1332-1347.
17. J.Q. Li, Z.F. Du, A two-stage fourth order time-accurate discretization for Lax-Wendroff type flow solvers I. hyperbolic conservation laws, *SIAM J. Sci. Computing*, 38 (2016) 3046-3069.
18. C. Liu, Y.J. Zhu, K. Xu, Unified gas-kinetic wave-particle methods I: Continuum and rarefied gas flow, *J. Comput. Phys.* 401 (2020) 108977.
19. R.B. Lowrie, A comparison of implicit time integration methods for non linear relaxation and diffusion, *J. Comput. Phys.* 196 (2004) 566-590.
20. R.G. McClarren, T.M. Evans, R.B. Lowrie, J.D. Densmore, Semi-implicit time integration for  $P_n$  thermal radiative transfer, *J. Comput. Phys.* 227 (2008) 7561-7586.
21. D. Mihalas, B. W. Mihalas, *Foundations of Radiation Hydrodynamics*, Oxford University Press (1984).
22. L. Pan, K. Xu, Q.B. Li, J.Q. Li, An efficient and accurate two-stage fourth-order gas-kinetic scheme for the Navier-Stokes equations, *J. Comput. Phys.* 326 (2016) 197-221.
23. G.C. Pomraning, *The Equations of Radiation Hydrodynamics*, Pergamon Press, Oxford (1973).
24. Y. Saad, M. H. Schultz, GMRES: A Generalized Minimal Residual Algorithm for Solving Nonsymmetric Linear Systems, *SIAM J. Sci. Comput.* 7 (1986) 856-869.
25. W.J. Sun, S. Jiang, K. Xu, An asymptotic preserving unified gas kinetic scheme for gray radiative transfer equations, *J. Comput. Phys.* 285 (2015) 265-279.
26. W.J. Sun, S. Jiang, K. Xu, S. Li, An asymptotic preserving unified gas-kinetic scheme for frequency-dependent radiative transfer equations, *J. Comput. Phys.* 302 (2015) 222-238.
27. W.J. Sun, S. Jiang, K. Xu, An implicit unified gas-kinetic scheme for radiative transfer with equilibrium and non-equilibrium diffusive limits, *Commun. Comput. Phys.* 22 (2015) 899-912.
28. W.J. Sun, S. Jiang, K. Xu, G.Y. Cao, Multiscale Simulation for the System of Radiation Hydrodynamics, *Journal of Scientific Computing* (2020) 85:25.
29. W.J. Sun, G.X. Ni, A pressure decoupled BGK model for the equations of radiation hydrodynamics, *Journal of Nanjing Normal University*, 36 (2013) 5-13.
30. H.Z. Tang, H.M. Wu, Kinetic flux vector splitting for radiation hydrodynamical equations. *Computers and Fluids* 29 (2000) 917-933.
31. K. Xu, A gas-kinetic BGK scheme for the Navier-Stokes equations and its connection with artificial dissipation and Godunov method, *J. Comput. Phys.* 171 (2001) 289-335.
32. K. Xu, *Direct modeling for computational fluid dynamics: construction and application of unified gas kinetic schemes*, World Scientific (2015).
33. K. Xu, J. Huang, A unified gas-kinetic scheme for continuum and rarefied flows, *J. Comput. Phys.* 229 (2010) 7747-7764.